

# Morphology dependent optical anisotropies in the n-type polymer P(NDI2OD-T2)

Steven J. Brown,<sup>1</sup> Ruth A. Schlitz,<sup>2</sup> Michael L. Chabinyo,<sup>1</sup> and Jon A. Schuller<sup>3</sup>

<sup>1</sup>*Materials Department, University of California, Santa Barbara, California 93106, United States*

<sup>2</sup>*SAGE Electrochromics, Inc., 2 Sage Way, Faribault, Minnesota 55021, United States\**

<sup>3</sup>*Electrical and Computer Engineering Department,  
University of California, Santa Barbara, California 93106, United States†*

(Dated: July 24, 2016)

Organic semiconductors tend to self-assemble into highly ordered and oriented morphologies with anisotropic optical properties. Studying these optical anisotropies provides insight into processing-dependent structural properties and informs the photonic design of organic photovoltaic and light-emitting devices. Here, we measure the anisotropic optical properties of spin-cast films of the n-type polymer P(NDI2OD-T2) using momentum-resolved absorption and emission spectroscopies. We quantify differences in the optical anisotropies of films deposited with distinct face-on and edge-on morphologies. In particular, we infer a substantially larger out-of-plane tilt angle of the optical transition dipole moment in high temperature annealed, edge-on films. Measurements of spectral differences between in-plane and out-of-plane dipoles, further indicate regions of disordered polymers in low temperature annealed face-on films that are otherwise obscured in traditional X-ray and optical characterization techniques. The methods and analysis developed in this work provide a way to identify and quantify subtle optical and structural anisotropies in organic semiconductors that are important for understanding and designing highly efficient thin film devices.

Organic semiconductors hold great promise in optoelectronic applications such as organic photovoltaics (OPVs)[1] and organic light emitting diodes (OLEDs)[2] due to their ease of processing (potentially leading to high-throughput and low-cost manufacture) and molecular tunability. Organic semiconductors typically self-assemble into highly ordered and oriented morphologies. As such, great strides have been made in characterizing and optimizing morphologies[3–7], with a particular focus on the electrical[8, 9] and optical[10–12] properties relevant to devices. As most morphologies are highly oriented, it is important to study the variation of these properties along different directions. For instance, anisotropic electrical properties of organic semiconductors directly impact charge transport[13–15] and must be accounted for in device design[16]. Optical spectroscopies such as ellipsometry[17, 18], polarized absorption[19], polarized photoluminescence[20], and Raman[21, 22], similarly reveal anisotropic optical properties related to the refractive index, absorption, emission, and vibrational modes that significantly impact the design and efficiency of light-emitting[23, 24] and photovoltaic[25, 26] devices.

Recently, momentum-resolved photoluminescence (mPL) measurements have provided new insight into magnetic dipoles in atomic systems[27], intra- and inter-molecular excitons in H-aggregates [28], and waveguide exciton polariton modes [29]. Here, we extend these techniques to study absorption as well as emission properties in highly ordered polymer films. We study the molecule P(NDI2OD-T2) which adopts distinct 'edge-on' or 'face-on' orientations depending

on processing conditions. By characterizing the optical anisotropies of both morphologies, we determine the average orientation of the transition dipoles, and resolve subtle differences in morphology (in both crystalline and non-crystalline regions). These results reveal structural features previously invisible to diffraction techniques and suggest ways to increase device performance through film morphology optimization.

P(NDI2OD-T2), sold by Polyera as N2200, is an n-type polymer. See Fig. 1(a) for its structural formula and Fig. 1(b,c) for geometry. As n-type semiconducting polymers are rare, P(NDI2OD-T2) has been the subject of extensive morphology[30–36] and charge transport[37–41] studies.

P(NDI2OD-T2) is a particularly interesting system for studies of structure-function relations because its molecular orientation can be controlled through processing. Annealing films at a low temperature (150°C) results in a face-on morphology where the pi-stacking direction is perpendicular to the substrate (see GIWAXS, Supplemental Material, Fig. S1).[42] In contrast, a high temperature anneal (305°C) results in an edge-on morphology with both the pi-stacking direction and polymer backbone parallel to the substrate.[43, 44] These two alternate morphologies are illustrated schematically in Fig. 1(d). Elucidating the effects various morphologies have on film function and device performance is on-going.

There have been a number of experiments linking processing conditions to optical properties. Previous optical studies of P(NDI2OD-T2) in various solvents as well as in thin films reveal subtle differences in absorption and photoluminescence (PL) spectra depending on the degree of aggregation.[45–47] Subsequent studies used rubbing, directional epitaxial crystallization, or epitaxy on oriented substrates to define a preferential in-plane alignment of the polymer chains.[19, 35] Polar-

\* Previous address: Materials Department, University of California, Santa Barbara, California 93106, United States

† jonschuller@ece.ucsb.edu

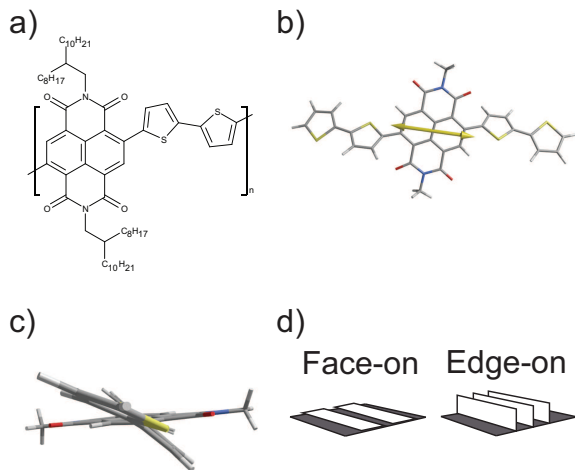


FIG. 1: a) The chemical structure of P(NDI2OD-T2). b) Geometry and transition dipole moment of a P(NDI2OD-T2) molecule, determined with DFT calculations. The transition dipole moment (yellow arrow) lies in the plane of the NDI unit and is angled slightly with respect to the backbone. The alkyl side-chains have been truncated for visibility. c) A view down the backbone showing the relative twist of thiophene units with respect to the NDI2OD unit. While the subunits are twisted for both isolated and crystalline polymer, the exact angle in the solid state is dependent on morphology. d) When annealed at 150°C or 305°C P(NDI2OD-T2) takes on a face-on or edge-on morphology, respectively. The planes shown refer to the orientation of the NDI2OD planes.

ized absorbance measurements then reveal in-plane optical anisotropies: the films primarily absorb light with electric fields polarized along the chain axis.[19, 35] These studies demonstrate significant optical structure-function relationships. However, these measurements of optical anisotropies require specialized processing techniques to achieve in-plane alignment and are insensitive to out-of-plane oriented optical properties. In this paper we use momentum-resolved spectroscopies to measure the anisotropic optical properties parallel vs. perpendicular to the substrate in films of P(NDI2OD-T2) deposited with standard processing conditions and exhibiting no preferred in-plane alignment over optical length scales.

## I. RESULTS AND DISCUSSION

### A. Momentum-resolved spectroscopy

Momentum-resolved spectroscopies are a suite of techniques particularly well-suited to measuring the orientation of emitters, absorbers, and scatterers. In these techniques, variations in, e.g., PL, absorption, reflection, or scattered light intensity are measured as a function

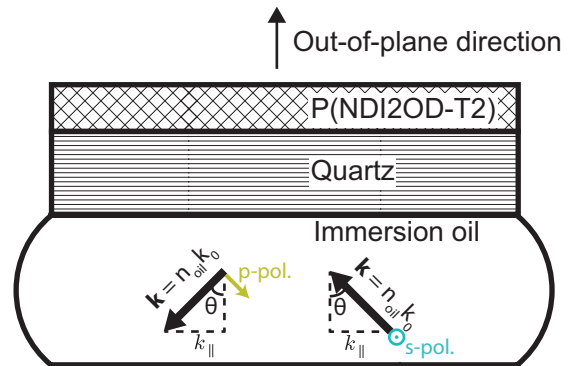


FIG. 2: Schematic showing the measurement geometry. In mPLE light is incident on the sample with a specific value of the in-plane momentum,  $k_{||}$ . In mPL light is emitted from the sample and measured as a function of  $k_{||}$ . The in-plane momentum is related to the angle of propagation as,  $k_{||} = n_{oil} k_0 \sin \theta$ . Both p-polarized and s-polarized light are independently measured for both techniques.

of the photon's momentum vector ( $\vec{k}$ ). These techniques utilize imaging in the back focal plane (Fourier plane) of a microscope objective (see Appendix A). Every point in the back focal plane corresponds to an angle of light incident on or emitted from the sample ( $\theta = \arcsin \frac{k_{||}}{n k_0}$ ,  $\phi = \arctan \frac{k_y}{k_x}$  where  $k_{||} = \sqrt{k_x^2 + k_y^2}$ ); see Fig. 2 for the measurement geometry. For example, in Fig. 3(a) we plot the p-polarized mPL from a thin film of P(NDI2OD-T2). Following previously established procedures, [28] we decompose mPL measurements like these into contributions from in-plane and out-of-plane oriented emission dipoles. Similarly, we also extend this basic technique to measure the orientation of *absorption* dipoles. Incident light is focused to a point in the back focal plane, Fig. 3(b), such that it impinges the sample at a specific angle. By moving this focused light source within the back focal plane, we have complete control of the incident photon momentum vector and can measure momentum-resolved absorption. Both PL and absorption measurements are analyzed with simple electromagnetic models, detailed below.

Because the emission (and absorption) distribution of a dipole is anisotropic ( $\propto \sin^2 \theta$ ), dipoles that are oriented in the plane of the sample (in-plane for the rest of the article) emit light into (or absorb light from) different angles than dipoles oriented perpendicular to the sample plane (out-of-plane). These differences are further amplified by reflections and interference in multi-layered geometries. Using a three-layer optical model, we calculate the p-polarized momentum-dependent PL intensity from purely in-plane (blue, solid) or out-of-plane (red, dashed) dipoles in a P(NDI2OD-T2) film, Fig. 4(a). The distributions are particularly different at normal incidence, where only in-plane (IP) dipoles emit, and at the critical angle,

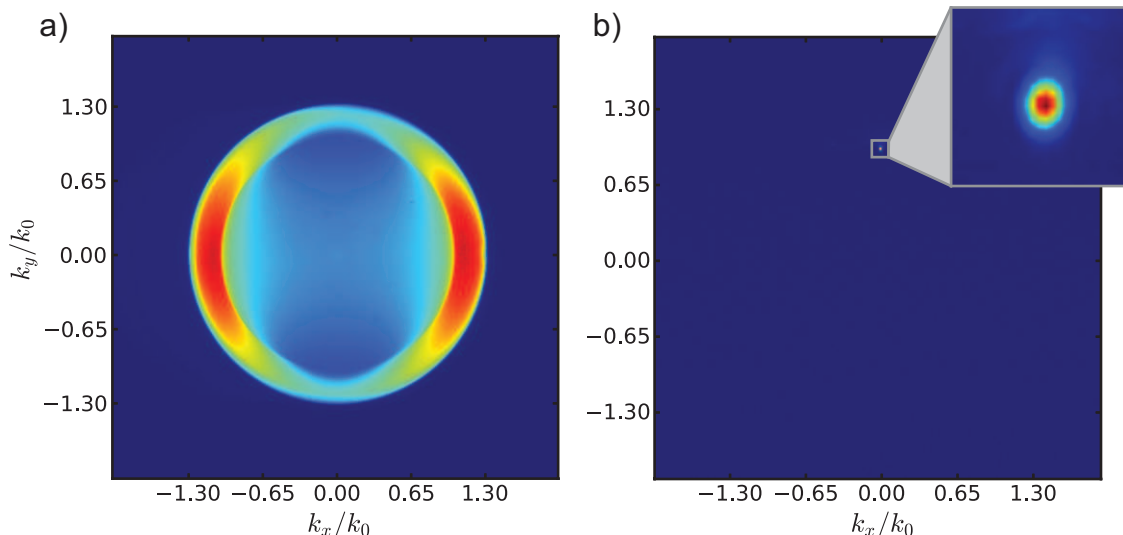


FIG. 3: (a) False color back focal plane image of y-polarized photoluminescence (750-1050nm integrated) from a P(NDI2OD-T2) film. Vertical (horizontal) linecuts through the center correspond to p-polarized (s-polarized) traces.

(b) False color back focal plane image of reflected laser light, demonstrating momentum-resolved excitation at  $k_x = -0.02k_0$ ,  $k_y = 0.96k_0$ . By moving the output laser fiber within this plane we control the incidence momentum vector of our excitation source. The inset is a magnified image of the laser spot.

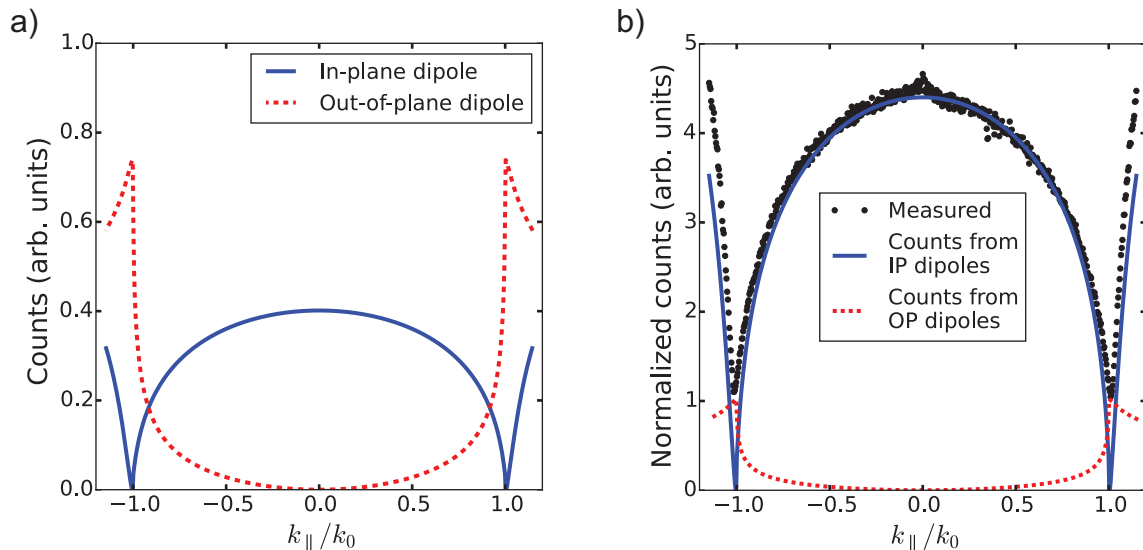


FIG. 4: (a) Calculated momentum-dependent p-polarized luminescence expected from equal magnitude in-plane (blue, solid) and out-of-plane (red, dashed) emitting dipoles. (b) P-polarized photoluminescence at 865nm of P(NDI2OD-T2) annealed at 150°C decomposed into counts due to in-plane and out-of-plane dipoles.

where only out-of-plane dipoles (OP) emit. We use these calculations to decompose measured momentum-resolved PL into contributions from IP and OP dipoles, Fig. 4(b). The 2D back focal plane PL image is focused to the entrance slit of an imaging spectrograph where it is separated spectrally. At each wavelength we measure the PL intensity as a function of in-plane momentum (black circles). The measured counts are decomposed into contributions from IP (blue, solid) and OP (red, dashed)

dipoles. In this case, 5 percent of the total PL counts originate from OP dipoles.

## B. Emission and absorption anisotropy

Measured (solid, dot-dashed) and calculated (dashed) p-polarized (yellow, solid) and s-polarized (cyan, dot-dash) 865 nm PL traces for face-on and edge-on films are

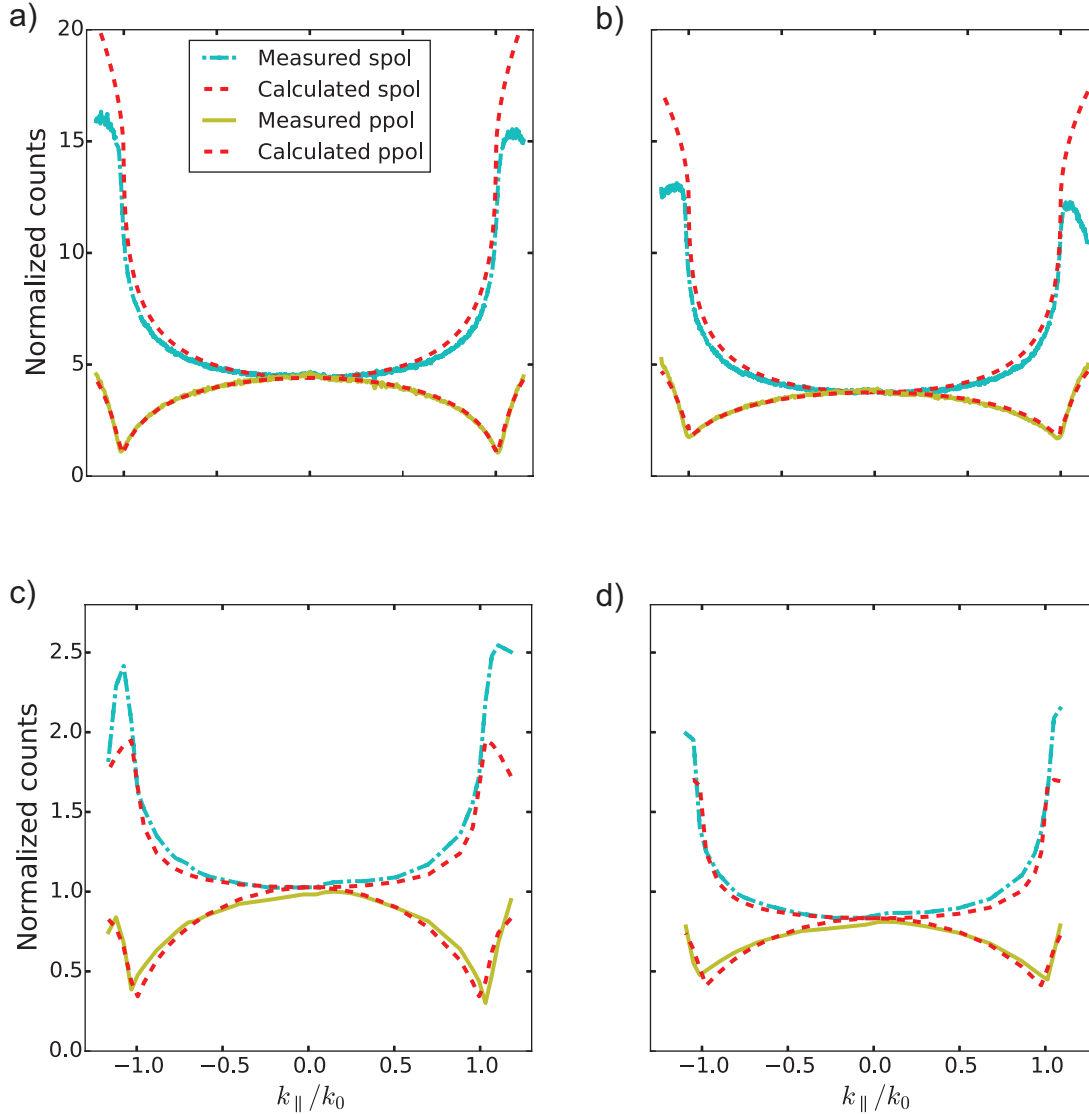


FIG. 5: Examples of mPL measurements: 865nm photoluminescence intensity is recorded (solid, dot-dashed lines) vs. emission momentum for (a) face-on and (b) edge-on P(NDI2OD-T2). P-polarized traces (yellow, solid) are fit (dashed lines) to determine the relative contribution of IP and OP dipoles as illustrated in figure 4. From these fits we determine a predicted shape of the s-pol data (cyan, dot-dashed) with no free fit-parameters. The ratio of OP to IP dipole moments is 0.13 and 0.29 for face-on and edge-on films respectively. Examples of mPLE measurements: total photoluminescence intensity is recorded vs. incident momentum of 700nm excitation laser for (c) face-on and (d) edge-on P(NDI2OD-T2). The curves exhibit visible differences from mPL due to different values of the experimental apodization factor and values of the refractive index at 700nm vs. 865nm (see Appendix A).  
Regardless, the fit results of mPLE (0.16 and 0.30) show excellent agreement with mPL.

shown in Figs. 5(a,b). The s-polarized calculations contain no free fit parameters and show excellent agreement with measured PL up to approximately  $k_{\parallel} = \pm 1.15 * k_0$ . This value of  $|k_{\parallel}|$  defines the range over which we perform fits of p-pol data—at larger momentum values the collection efficiency of the microscope objective begins to drop. The p-polarized experimental traces are fit according to the calculations described above, providing a measure of the relative contribution of in-plane and out-

of-plane dipoles. As expected for excitations oriented primarily along the polymer chain, the emission in both morphologies is dominated by an in-plane dipole moment. However, fits of the p-polarized PL traces reveal a significant difference between the two morphologies. The ratio of out-of-plane to in-plane dipole moments is more than twice as large for edge-on (0.29) than face-on (0.13) morphologies. mPL allows us to resolve differences in the optical anisotropies that are *not* evident in ellipsometry

(Supplemental Material, Fig. S2).[42]

From mPL we derive the orientation of the transition dipole moment (TDM) with respect to the substrate. The ratio of OP to IP dipole moments translate into differences of the average inclination angle of the TDM with respect to the substrate. The inferred angle is  $\arctan(0.13) = 7^\circ$  for face-on films compared to  $\arctan(0.29) = 16^\circ$  for edge-on orientations. This increase in angle is consistent with the orientation of NDI planes in face-on versus edge-on films. DFT calculations indicate a TDM is oriented mostly, but not completely, parallel to the polymer backbone. The TDM is tilted ( $8^\circ$ ) in the NDI plane, see Fig. 1(b).[33, 37, 38] In the edge-on morphology, the TDM is thus partially aligned perpendicular to the substrate. There may also be a tilting of the polymer backbone with respect to the substrate.[48] and we cannot unambiguously identify the cause of differences in TDM orientation between the two morphologies. It is worth noting that the optical technique used here averages both crystalline and amorphous regions and therefore provides different information than can be found from X-ray diffraction alone.

From Lorentz reciprocity[49], momentum-resolved light absorption is formally equivalent to momentum-resolved emission. Using the same principles described above, we provide the first demonstrations of momentum-resolved photoluminescence excitation (mPLE), a proxy for absorption (assuming photoluminescence intensity is linearly proportional to the amount of light absorbed). We collect the total emitted PL (integrated over wavelength and momentum) as a function of the position of our momentum-resolved laser excitation source, Fig. 2(b). Face-on and edge-on mPLE measurements are plotted in Figs. 5(c) and (d) at an excitation wavelength of 700 nm. Fitting these traces to the appropriate in-plane and out-of-plane basis functions at 700 nm (see Appendix C), we find out-of-plane to in-plane ratios of 0.16 and 0.30 for face-on and edge-on morphologies respectively. This excellent agreement with momentum-resolved emission (0.13 and 0.29) further validates our observation of larger TDM tilt-angles for edge-on polymer films. This also indicates minimal reorientation of the transition dipole between absorption and emission processes as can occur in other systems.[50–52]

### C. Spectral differences

The wavelength dependence of these momentum-resolved measurements provides additional insight into the differences in optical properties for the two film morphologies. We only determine mPLE (i.e., absorption) at an excitation wavelength of 700 nm. The emitted light, on the other hand, is separated by momentum and wavelength simultaneously. Performing decompositions similar to Fig. 4(b), we observe an average OP/IP ratio of 0.12 with a standard deviation of 0.1 across the PL band (750-1050nm) for face-on films. Although the ratio

is *mostly* constant across the PL spectrum, deviations from these values are observed primarily at wavelengths to the right of the PL peak. This deviation is most easily visualized by plotting the normalized IP and OP spectra inferred from our fits at each wavelength. For face-on films, Fig. 6(a), the s-polarized spectrum (light green), which arises from only IP dipoles, is in close agreement with the IP spectrum determined from fits of p-polarized data (blue, solid). In particular, both spectra reveal a shoulder feature at 950 nm that is absent from the OP spectrum (red, dashed) determined from our fits. In comparison, edge-on films, Fig. 6(b) show much closer agreement between all three spectra (the out-of-plane artifact past 1000nm is due to low PL counts throwing off the fitting procedure). Evidently, the spectral dependence of these optical anisotropies reveals subtle differences in the morphology-dependent optical properties that are otherwise obscured.

In previous studies, this 950nm shoulder peak was only seen in aggregated P(NDI2OD-T2).[45]. A likely explanation for the missing face-on shoulder peak is that out-of-plane oriented dipoles are preferentially found in amorphous regions of the sample. When the polymer is initially spin-cast onto the substrate most of the molecules aggregate and align in the plane of the substrate. Some molecules, however, will exist in amorphous regions where there is a more random orientation of the molecules. The low temperature anneal provides only a small amount of energy for the molecules to rearrange and very little of the amorphous regions will crystallize. In this scenario out-of-plane dipoles are preferentially found in these randomly oriented amorphous regions. In contrast, a high temperature anneal, which gives rise to the edge-on morphology, has much more energy for the molecules to adjust and crystallize. A large portion of the amorphous polymers will crystallize while mostly retaining their original orientation. This simple model likely explains why the 950nm shoulder peak is found in the out-of-plane spectra for edge-on, but not face-on, morphologies.

## II. CONCLUSION

In conclusion we use momentum-resolved spectroscopies to measure in-plane and out-of-plane effective dipole moments for face-on and edge-on morphologies of P(NDI2OD-T2). Fits of momentum-resolved emission measurements (mPL) show close agreement with first-ever analogous absorption measurements using a momentum-resolved photoluminescence excitation (mPLE) technique. We find that edge-on films exhibit a larger out-of-plane tilt angle ( $\sim 16^\circ$ ) of the transition dipole moment relative to face-on films ( $\sim 7^\circ$ ). These results are consistent with the orientation of the transition dipole moment within NDI planes, but may alternatively be indicative of a difference in average orientation of the polymer backbones. We also observe a missing

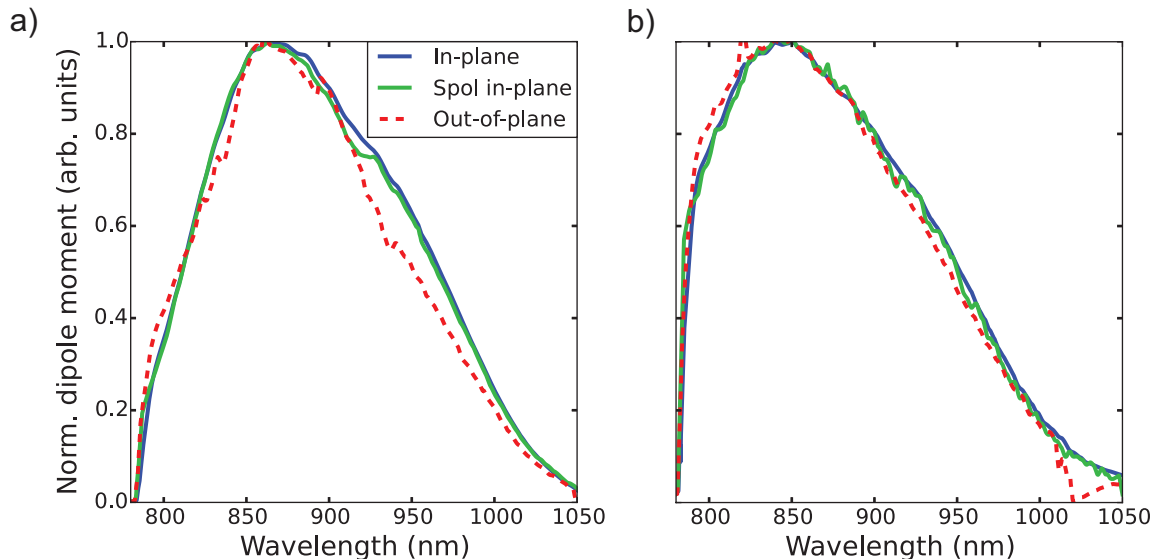


FIG. 6: In-plane and out-of-plane normalized emission dipole moments for (a) face-on and (b) edge-on P(NDI2OD-T2), determined by performing mPL decompositions across the entire 780-1050 nm emission band.

shoulder peak, characteristic of aggregated P(NDI2OD-T2), in the out-of-plane emission spectrum of face-on films. This suggests that the out-of-plane emission in these films arises largely from amorphous regions. As typical optical techniques only measure in-plane oriented dipoles and X-ray diffraction only measures crystalline regions of the film, these out-of-plane amorphous regions have likely been unexplored in previous studies. Finding annealing techniques that maintain face-on orientation while crystallizing these previously hidden regions will likely lead to better charge transport and, therefore, device performance in organic photovoltaics and light-emitting diodes. In addition to these insights on P(NDI2OD-T2)'s morphology, the momentum-resolved techniques developed in this paper can be used to accurately characterize anisotropic optical properties in other materials. These techniques can therefore enable new optimizations of optical device design and reveal subtle differences in morphology that are obscured in other X-ray and optical characterization techniques.

#### ACKNOWLEDGMENTS

This work was supported by a National Science Foundation CAREER award (DMR-1454260). AFM and UV-Vis spectroscopy were performed in the MRL Shared Experimental Facilities which are supported by the MRSEC Program of the NSF under Award No. DMR 1121053; a member of the NSF-funded Materials Research Facilities Network ([www.mrfln.org](http://www.mrfln.org)). A portion of this work was performed in the UCSB Nanofabrication Facility.

#### Appendix A: Experimental setup

By placing a detector in the back focal plane of a microscope objective, Fig. 7,[42] we separate light based on the angle, or momentum, at which it leaves the sample. A spectrometer (Princeton Instruments IsoPlane SCT320) coupled to a 2D CCD camera (Princeton Instruments PIXIS 1024BRX) separates light by wavelength along one axis of the camera and momentum along the other axis. This allows measurements of momentum-dependent photoluminescence intensity at many wavelengths simultaneously. From this data, we separate emission spectra from dipoles oriented in-plane and out-of-plane. For mPL experiments we used a collimated LED source (ThorLabs M735L3-C5) to excite the sample across all momenta uniformly.

Similarly to how placing a detector in a conjugate back focal plane to the objective allowed us to study emission of different momenta of light, we placed our excitation source in another conjugate back focal plane to study absorption as a function of light momenta. We studied absorption properties by measuring the integrated intensity of photoluminescence emitted from the sample versus the input excitation momentum (similar to how photoluminescence excitation, or PLE, measures PL versus input wavelength of light). The end of a single mode optical fiber (coming from a fiber-coupled supercontinuum source (SuperK Extreme EXR-15)) was mounted on a translation stage. By moving the end of the fiber within the conjugate back focal plane, we control the incident momentum vector of the light exciting the sample.

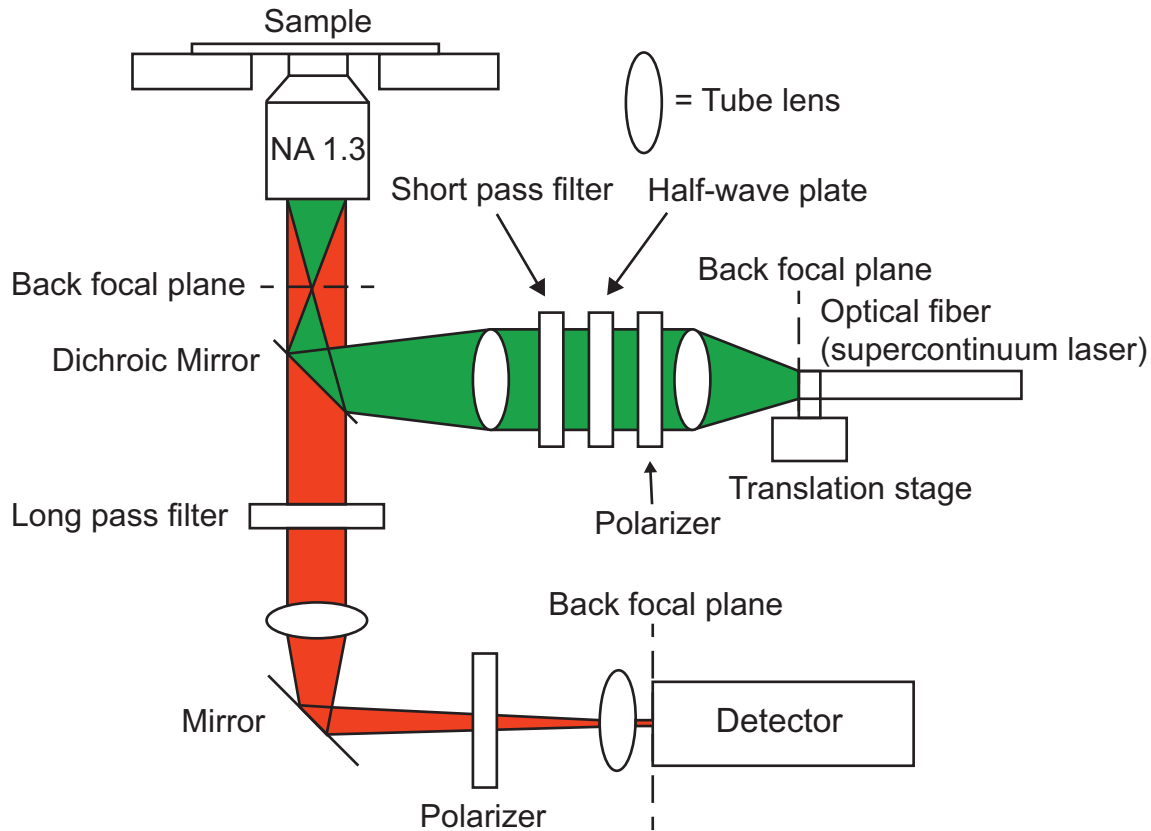


FIG. 7: The momentum-resolved setup used in the experiments. For momentum-resolved photoluminescence, the supercontinuum excitation source along with the half-wave plate, polarizer, and first tube lens were replaced with a collimated LED.

### Appendix B: Sample fabrication

P(NDI2OD-T2) (Polyera ActivInk N2200) was spin-cast from 1,2-dichlorobenzene solution (10  $\mu\text{g}/\text{mL}$ ). Samples were then annealed at 150  $^{\circ}\text{C}$  for one hour to produce face-on samples or at 305  $^{\circ}\text{C}$  for one hour to produce edge-on samples. The samples were then allowed to slowly cool to room temperature. Film thickness was measured using atomic force microscopy (AFM). Glass, 200nm silicon dioxide on silicon, and quartz coverslip substrates were used for AFM, ellipsometry, and PL measurements respectively.

### Appendix C: Data analysis

Raw camera images were analyzed using Python. In mPL we obtain a rectangular image with wavelength varying along the x-axis and momentum varying along the y-axis. To obtain in-plane and out-of-plane emission dipole moments we analyzed each wavelength independently. For a given wavelength column in the p-polarized image, we first converted the pixels of the camera into units of  $k_0$  by setting the edges of PL to the 1.3 NA ( $\pm 1.3k_0$ ) of our microscope objective. After convert-

ing to units of momentum we used a three layer model (following the treatment in Schuller *et al.*[28]) to solve for the linear combination of in-plane and out-of-plane effective emission dipole moments that summed to the intensity vs. momentum shape measured at each wavelength. The model's input parameters—refractive index and film thickness—were determined from ellipsometry and AFM measurements respectively. After fitting p-polarized data, we determine the expected s-polarized PL intensity vs. momentum and compare to actual s-polarized measurements.

Data analysis for mPLE was similar, but had many separate images that needed to be aggregated. For each PL image the exciting laser y-position was determined by taking the image of the reflected laser spot without the PL filter. Each PL image was background subtracted using a "window frame" of dark pixels that surrounded the pixels receiving PL in the center of the image. This allowed us to correct for background drift over time. The background subtracted PL image was then summed across all pixels to determine a single PL value for each image. From the PL image we were able to convert pixels to  $k_0$  as above. We then found the linear combination of in-plane and out-of-plane effective absorption dipole moments that summed to the counts vs. momentum shape

observed. Again, we determine the expected s-polarized PL intensity vs. incident momentum and compare to actual s-polarized measurements. It is important to note that while the mPL model includes an apodization factor, given the setup geometry the mPLE model does not. In mPL, each pixel of fixed width in the back-focal-plane correspond to a different magnitude of solid-angle over which the PL is collected. Thus, an isotropic emitter would still exhibit intensity variations across the back focal plane image. In mPLE, the solid-angle magnitude also changes, but the input power is fixed and no correction is needed.

Dipole moments found via mPL and mPLE are highly sensitive to the film refractive indices input in the three-layer model (especially in the out-of-plane direction). For this reason it is essential to have accurate optical constants. We used atomic force microscopy, UV-Vis transmission, and ellipsometry to get accurate thickness, in-plane extinction coefficient, and refractive indices respectively.

- [1] K. A. Mazzio and C. K. Luscombe, *Chem. Soc. Rev.* **44**, 78 (2014).
- [2] L. S. Hung and C. H. Chen, *Materials Science and Engineering: R: Reports* **39**, 143 (2002).
- [3] D. M. DeLongchamp, R. J. Kline, D. A. Fischer, L. J. Richter, and M. F. Toney, *Advanced Materials* **23**, 319 (2011).
- [4] D. M. DeLongchamp, R. J. Kline, E. K. Lin, D. A. Fischer, L. J. Richter, L. A. Lucas, M. Heeney, I. McCulloch, and J. E. Northrup, *Adv. Mater.* **19**, 833 (2007).
- [5] N. D. Treat, J. A. Nekuda Malik, O. Reid, L. Yu, C. G. Shuttle, G. Rumbles, C. J. Hawker, M. L. Chabiny, P. Smith, and N. Stingelin, *Nat Mater* **12**, 628 (2013).
- [6] Y. Diao, B. C.-K. Tee, G. Giri, J. Xu, D. H. Kim, H. A. Becerril, R. M. Stoltenberg, T. H. Lee, G. Xue, S. C. B. Mannsfeld, and Z. Bao, *Nat Mater* **12**, 665 (2013).
- [7] B.-G. Kim, E. J. Jeong, J. W. Chung, S. Seo, B. Koo, and J. Kim, *Nat Mater* **12**, 659 (2013).
- [8] R. Noriega, J. Rivnay, K. Vandewal, F. P. V. Koch, N. Stingelin, P. Smith, M. F. Toney, and A. Salleo, *Nat Mater* **12**, 10388 (2013).
- [9] D. Venkateshvaran, M. Nikolka, A. Sadhanala, V. Lemaur, M. Zelazny, M. Kepa, M. Hurhangee, A. J. Kronemeijer, V. Pecunia, I. Nasrallah, I. Romanov, K. Broch, I. McCulloch, D. Emin, Y. Olivier, J. Cornil, D. Beljonne, and H. Sirringhaus, *Nature* **515**, 384 (2014).
- [10] J. Cabanillas-Gonzalez, G. Grancini, and G. Lanzani, *Advanced Materials* **23**, 5468 (2011).
- [11] F. C. Spano, *Acc. Chem. Res.* **43**, 429 (2010).
- [12] B. J. Schwartz, *Annual Review of Physical Chemistry* **54**, 141 (2003).
- [13] V. C. Sundar, J. Zaumseil, V. Podzorov, E. Menard, R. L. Willett, T. Someya, M. E. Gershenson, and J. A. Rogers, *Science* **303**, 1644 (2004).
- [14] C. Reese and Z. Bao, *Adv. Mater.* **19**, 4535 (2007).
- [15] H. Sirringhaus, P. J. Brown, R. H. Friend, M. M. Nielsen, K. Bechgaard, B. M. W. Langeveld-Voss, A. J. H. Spiering, R. a. J. Janssen, E. W. Meijer, P. Herwig, and D. M. d. Leeuw, *Nature* **401**, 685 (1999).
- [16] M. Shah, V. Pryamitsyn, and V. Ganesan, *Applied Physics Letters* **95**, 194101 (2009).
- [17] M. Campoy-Quiles, P. G. Etchegoin, and D. D. C. Bradley, *Phys. Rev. B* **72**, 045209 (2005).
- [18] M. Campoy-Quiles, J. Nelson, P. G. Etchegoin, D. D. C. Bradley, V. Zhokhavets, G. Gobsch, H. Vaughan, A. Monkman, O. Ingnas, N. K. Persson, H. Arwin, M. Garriga, M. I. Alonso, G. Herrmann, M. Becker, W. Scholdei, M. Jahja, and C. Bubeck, *physica status solidi (c)* **5**, 1270 (2008).
- [19] K. Tremel, F. S. U. Fischer, N. Kayunkid, R. D. Pietro, R. Tkachov, A. Kiriy, D. Neher, S. Ludwigs, and M. Brinkmann, *Adv. Energy Mater.* **4** (2014), 10.1002/aenm.201301659.
- [20] C. Soci, D. Comoretto, F. Marabelli, and D. Moses, *Phys. Rev. B* **75**, 075204 (2007).
- [21] D. T. James, B. K. C. Kjellander, W. T. T. Smaal, G. H. Gelinck, C. Combe, I. McCulloch, R. Wilson, J. H. Burroughes, D. D. C. Bradley, and J.-S. Kim, *ACS Nano* **5**, 9824 (2011).
- [22] S. Kotarba, J. Jung, A. Kowalska, T. Marszalek, M. Kozanecki, P. Miskiewicz, M. Mas-Torrent, C. Rovira, J. Veciana, J. Puigmarti-Luis, and J. Ulanski, *Journal of Applied Physics* **108**, 014504 (2010).
- [23] T. D. Schmidt, D. S. Setz, M. Flmmich, J. Frischeisen, D. Michaelis, C. Mayr, A. F. Rausch, T. Wehlus, B. J. Scholz, T. C. G. Reusch, N. Danz, and W. Brtting, *Applied Physics Letters* **103**, 093303 (2013).
- [24] M. Grell and D. D. C. Bradley, *Adv. Mater.* **11**, 895 (1999).
- [25] S. B. Jo, H. H. Kim, H. Lee, B. Kang, S. Lee, M. Sim, M. Kim, W. H. Lee, and K. Cho, *ACS Nano* **9**, 8206 (2015).
- [26] R. R. Grote, S. J. Brown, J. B. Driscoll, R. M. Osgood, and J. A. Schuller, *Opt. Express* **21**, A847 (2013).
- [27] T. H. Taminiau, S. Karaveli, N. F. van Hulst, and R. Zia, *Nat Commun* **3**, 979 (2012).
- [28] J. A. Schuller, S. Karaveli, T. Schiros, K. He, S. Yang, I. Kymissis, J. Shan, and R. Zia, *Nat Nano* **8**, 271 (2013).
- [29] T. Ellenbogen and K. B. Crozier, *Phys. Rev. B* **84**, 161304 (2011).
- [30] C. J. Takacs, N. D. Treat, S. Krmer, Z. Chen, A. Facchetti, M. L. Chabiny, and A. J. Heeger, *Nano Lett.* **13**, 2522 (2013).
- [31] E. Gann, C. R. McNeill, M. Szumilo, H. Sirringhaus, M. Sommer, S. Maniam, S. J. Langford, and L. Thomsen, *The Journal of Chemical Physics* **140**, 164710 (2014).
- [32] E. Giussani, D. Fazzi, L. Brambilla, M. Caironi, and C. Castiglioni, *Macromolecules* **46**, 2658 (2013).
- [33] N. Martino, D. Fazzi, C. Sciascia, A. Luzio, M. R. Antognazza, and M. Caironi, *ACS Nano* **8**, 5968 (2014).
- [34] T. Schuettfort, L. Thomsen, and C. R. McNeill, *J. Am. Chem. Soc.* **135**, 1092 (2013).
- [35] M. Brinkmann, E. Gonthier, S. Bogen, K. Tremel, S. Ludwigs, M. Hufnagel, and M. Sommer, *ACS Nano* **6**, 10319 (2012).
- [36] A. M. Anton, R. Steyrlleuthner, W. Kossack, D. Neher, and F. Kremer, *Macromolecules* **49**, 1798 (2016).
- [37] D. Fazzi and M. Caironi, *Phys. Chem. Chem. Phys.* **17**, 8573 (2015).
- [38] M. Caironi, M. Bird, D. Fazzi, Z. Chen, R. Di Pietro, C. Newman, A. Facchetti, and H. Sirringhaus, *Adv. Funct. Mater.* **21**, 3371 (2011).
- [39] S. Fabiano, H. Yoshida, Z. Chen, A. Facchetti, and M. A. Loi, *ACS Appl. Mater. Interfaces* **5**, 4417 (2013).
- [40] V. D’Innocenzo, A. Luzio, A. Petrozza, D. Fazzi, and M. Caironi, *Adv. Funct. Mater.* **24**, 5584 (2014).
- [41] A. Luzio, L. Criante, V. D’Innocenzo, and M. Caironi, *Sci. Rep.* **3** (2013), 10.1038/srep03425.
- [42] See Supplemental Material for grazing incidence wide-angle X-ray scattering (GIWAXS) of face-on and edge-on P(NDI2OD-T2); ellipsometry of face-on and edge-on P(NDI2OD-T2).
- [43] J. Rivnay, R. Steyrlleuthner, L. H. Jimison, A. Casadei, Z. Chen, M. F. Toney, A. Facchetti, D. Neher, and A. Salleo, *Macromolecules* **44**, 5246 (2011).
- [44] T. Schuettfort, S. Huettner, S. Lilliu, J. E. Macdonald, L. Thomsen, and C. R. McNeill, *Macromolecules* **44**, 1530 (2011).
- [45] R. Steyrlleuthner, M. Schubert, I. Howard, B. Klaumzner, K. Schilling, Z. Chen, P. Saalfrank, F. Laquai, A. Fac-

- chetti, and D. Neher, *J. Am. Chem. Soc.* **134**, 18303 (2012).
- [46] E. Pavlopoulou, C. S. Kim, S. S. Lee, Z. Chen, A. Facchetti, M. F. Toney, and Y.-L. Loo, *Chem. Mater.* **26**, 5020 (2014).
- [47] N.-K. Kim, S.-Y. Jang, G. Pace, M. Caironi, W.-T. Park, D. Khim, J. Kim, D.-Y. Kim, and Y.-Y. Noh, *Chem. Mater.* **27**, 8345 (2015).
- [48] E. Giussani, L. Brambilla, D. Fazzi, M. Sommer, N. Kayunkid, M. Brinkmann, and C. Castiglioni, *J. Phys. Chem. B* **119**, 2062 (2015).
- [49] R. J. Potton, *Rep. Prog. Phys.* **67**, 717 (2004).
- [50] A. Montali, C. Bastiaansen, P. Smith, and C. Weder, *Nature* **392**, 261 (1998).
- [51] M. Forster, D. Thomsson, P. R. Hania, and I. G. Scheblykin, *Phys. Chem. Chem. Phys.* **9**, 761 (2007).
- [52] B. J. Schwartz, T.-Q. Nguyen, J. Wu, and S. H. Tolbert, *Synthetic Metals* **116**, 35 (2001).

## Supplemental Materials: Morphology dependent optical anisotropies in the n-type polymer P(NDI2OD-T2)

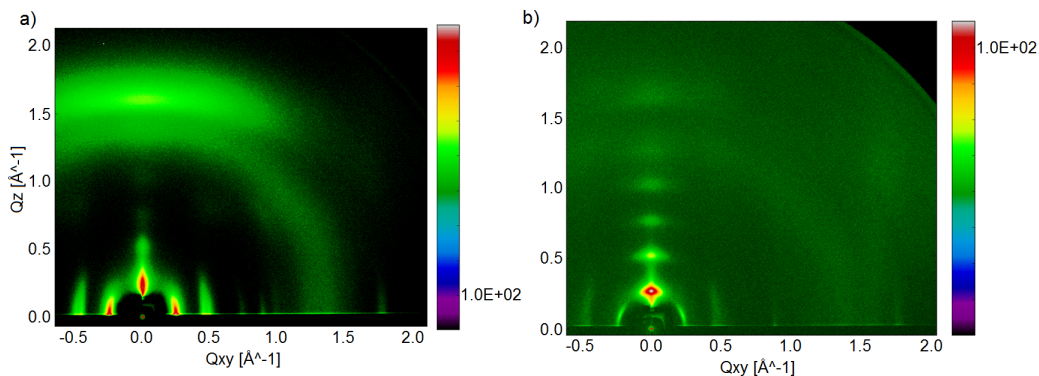


FIG. S1: a) Grazing incidence wide-angle X-ray scattering (GIWAXS) for a face-on oriented P(NDI2OD-T2) annealed at 150°C for 6 hours and b) for an edge-on oriented P(NDI2OD-T2) annealed at 300°C for 45 minutes.

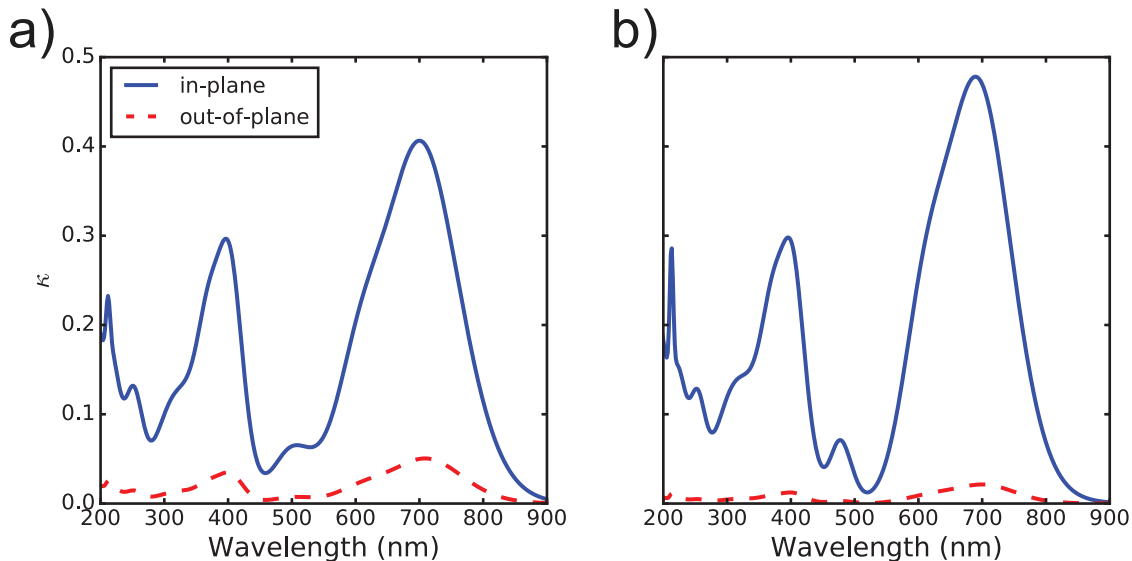


FIG. S2: The extinction coefficient in the in-plane and out-of-plane directions (with respect to the substrate) for (a) face-on and (b) edge-on P(NDI2OD-T2), determined from spectroscopic ellipsometry measurements. The ellipsometry results are highly model dependent and unable to capture the differences in optical anisotropies that are evident in momentum-resolved measurements.